Stony Brook University

Systematic Study of Elliptic Flow in Au+Au Collisions at $\sqrt{s_{NN}} = 200GeV$

A Thesis Presented By

Stanislav Salnikov

to

The Graduate School

in Partial Fulfillment of the

Requirements for the Degree of

Master of Science

in

Chemistry

Stony Brook University

August 2010

Stony Brook University

The Graduate School

Stanislav Salnikov

We, the thesis committee for the above candidate for the Master of Science degree, hereby recommend acceptance of this thesis.

Roy Lacey - Thesis Advisor

Professor, Department of Chemistry

Jiangyong Jia - Chair

Assistant Professor, Department of Astronomy and Physics

Fernando Raineri

Professor, Department of Chemistry

This thesis is accepted by the Graduate School

Lawrence Martin

Dean of the Graduate School

Abstract of the Thesis

Systematic Study of Elliptic Flow in Au+Au Collisions at $\sqrt{s_{NN}} = 200GeV$

by

Stanislav Salnikov

Master of Science

in

Chemistry

Stony Brook University

2010

Ultra-relativistic heavy ion collisions provide a unique opportunity for study of a new state of matter known as the Quark Gluon Plasma (QGP) under laboratory conditions. The Relativistic Heavy Ion Collider (RHIC) at Brookhaven National Laboratory is an accelerator designed to create and study such plasma. The azimuthal anisotropy of particle production in these collisions is a unique tool for studying the properties of the QGP. It is quantified by the second harmonic v_2 of the Fourier expansion of the azimuthal distribution of emitted particles. This elliptic flow is created by pressure gradients caused by the geometrical anisotropy of the initial collision zone, and transformed into momentum anisotropy of produced particles during the hydrodynamic expansion of the QGP medium. In this study, precision measurements of v_2 are presented for data collected by the PHENIX detector for Au+Au collisions at $\sqrt{s_{NN}}$ = 200 GeV in Run 7. The measurements are performed for charged hadrons with transverse momentum of 0.4 - 1.95 GeV/c, for the collision centrality

range 0-50%. To study the influence of non-flow effects, measurements were also obtained with event planes separated from the PHENIX central arms by different pseudorapidity gaps ($\triangle\eta$). The v_2 measurements indicate large values of v_2 which are compatible with QGP formation in Au+Au collisions at $\sqrt{s_{NN}} = 200$ GeV. Measurements for event planes with $\triangle\eta > 1$ show results which are consistent with each other, suggesting a negligible role for non-flow effects in the momentum and centrality range used in this analysis. Detailed comparisons of the v_2 measurements obtained with different event planes, as well as comparisons to the results obtained by the STAR collaboration, indicate overall good agreement; relatively small differences in the most central collisions can be understood in terms of a systematic uncertainty in the centrality estimates by the PHENIX and STAR experiments. The precision measurements presented here provide an important experimental basis for reliable extraction of QGP transport coefficients such as viscosity from v_2 measurements.

Contents

List of Figures

Acknowledgements

First and foremost, I would like to thank the people who guided me through my work towards this thesis, especially my advisor, Dr. Roy Lacey. Professor Lacey has always been patient and given me good advice about the work. He has been a great inspiration and provided lots of encouragement in the days of work. I would like to thank Dr. Jiangyong Jia for his example of great work and for being someone students might aspire to become one day. I am very grateful also to Dr. Fernando Raineri for all the great support he offered throughout my time in Stony Brook.

A special word of thanks goes to Dr. Arkadij Taranenko for his help and professional advice on the details of research. I would like to thank my fellow graduate students- Damian Reynolds, Somya Mohapatra, Xiaoyang Gong, Alex Mwai, Marcelo Nomura and the others for the moral support in the days of duress and for the many helpful hints and advice they had given me on the work. I give a special word of thanks to Tiffany Red, who has always kept up my spirits and optimism. Last, but not least, I would like to thank the PHENIX Collaboration for showing me how the scientific community works.

1 Introduction and Motivation

1.1 Introduction

The matter that we commonly interact with in everydays world is known to consist of atoms. Atoms have been found to consist of nuclei and electrons, and nuclei to be composed of the particles known as hadrons. However, hadrons are thought to be composite states themselves, made of particles named quarks and gluons. The theory that describes the behavior and interaction of those particles is known as Quantum Chromodinamics (QCD). However, QCD also tells us that quarks and gluons cannot be observed as independent particles, therefore, leading to searches for alternate ways to probe their properties.

The main goal of heavy ion collision experiments at Brookhaven National Lab's RHIC (Relativistic Heavy Ion Collider) is to study the new state of matter called QGP (Quark-Gluon Plasma). In this state, quarks and gluons (commonly called "partons") are deconfined over a space that is larger than the general size of a hadron. Generally, quarks and gluons are confined within composite states known as hadrons, however, at a high energy density, local deconfinement might occur, creating states of matter where quarks and gluons are the degrees of freedom. Just as at high temperature electrons can dissociate from atoms, forming a state of matter called plasma, at the extreme temperature/pressure conditions nucleons might break apart into their constitutients forming the quark-gluon plasma. In nature, such a state is believed to have existed at the earliest stages of development of the Universe, just a few microseconds from the beginning of the Big Bang, and might also exist in the highest-energy processes that occur in the Universe nowadays. The significance of studying such a state of matter covers such diverse regions of science as astrophysics, particle physics and quantum theory of strong interaction. Colliding heavy nuclei at ultrarelativistic

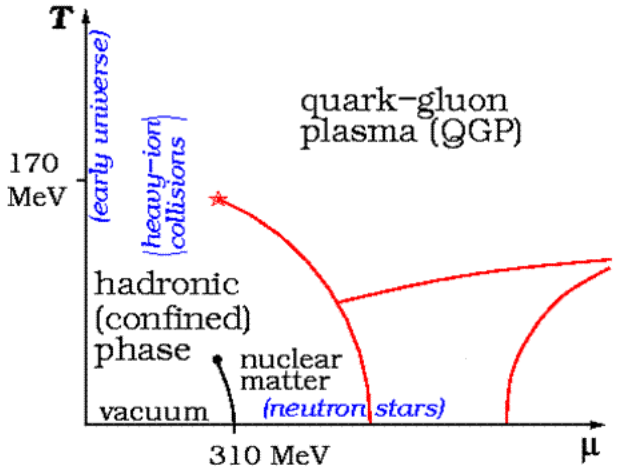

Figure 1: The QCD Phase Diagram.

velocities is a way to create and study such matter in the lab on Earth. Current experiments at RHIC involve Au-Au collisions with $\sqrt{s_{NN}} = 200$ GeV.

Figure 1 shows the schematic phase diagram for the nuclear matter, with the different possible phases labeled and red lines showing the phase transitions between those states. At the normal (labeled as "nuclear matter" on the diagram) temperatures and densities, quarks are confined within the nucleons. However, when the temperature is large enough, so that quark separation increases beyond a scale of 1 fm (approximately the diameter of a nucleon) and/or the pressure is large enough to "crush" the nuclei into their constituents, a phase might be observed with quarks and gluons as degrees of freedom. At the diagram, we can see several regions of different state of matter where that might happen. The heavy-ion collisions aim to investigate the high-temperature, low chemical potential zone of the QCD phase diagram (Fig.1).

1.2 Collision

In order to produce and study such a state of matter as QGP, extreme temperatures (of an order of more than 10^12 K or more than 170 MeV) is required. Heavy ion collisions are the

only known way to create such conditions in the lab. Heavy nuclei are accelerated to very large velocities (99.95% of the speed of light) and collided, creating a region with extreme energy density. The process of collision creates a very miniscule amount of matter, and that matter exists on a very short timescale before decomposing into more conventional particles. Figure 2 shows the space-time evolution of the collision processes. At the initial phase of the collision, large amount of partons are produced within a small volume via scattering between the participant nucleons. Through the consequent re-scatterings, the partons reach local equilibrium in a process known as thermalisation. The thermalised matter expands and cools, until at some point it reaches critical temperature T_c and undergoes a phase transition into a gas of conventional, colorless particles (hadron gas). This moment is called "chemical freezout", signifying the end of partonic phase and parton-parton interactions. Another important point of time is kinetic freezout - the point where the separation between the particles in the hadron gas grows large enough to prevent further interaction between them. After the kinetic freezout, the produced hadrons and other particles are free to fly away to be detected. Considering the short lifetime of the system, the conventional probes aren't an option, and the matter is studied by investigating the products of its decomposition. A large amount of various particles is produced in a collision and can be measured by the detector. The detector PHENIX (Pioneering High Energy Nuclear Interaction Experiment) at RHIC is one of the instruments dedicated to such studies. There are several probes that can give us information on the matter. One of the probes is the anisotropy of the produced particles.

1.3 Azimuthal Anisotropy

The anisotropy of particle production results from the geometry of the collision (Fig.3). Indeed, if one looks at the shapes of two colliding nuclei, one can realise that the shape of the

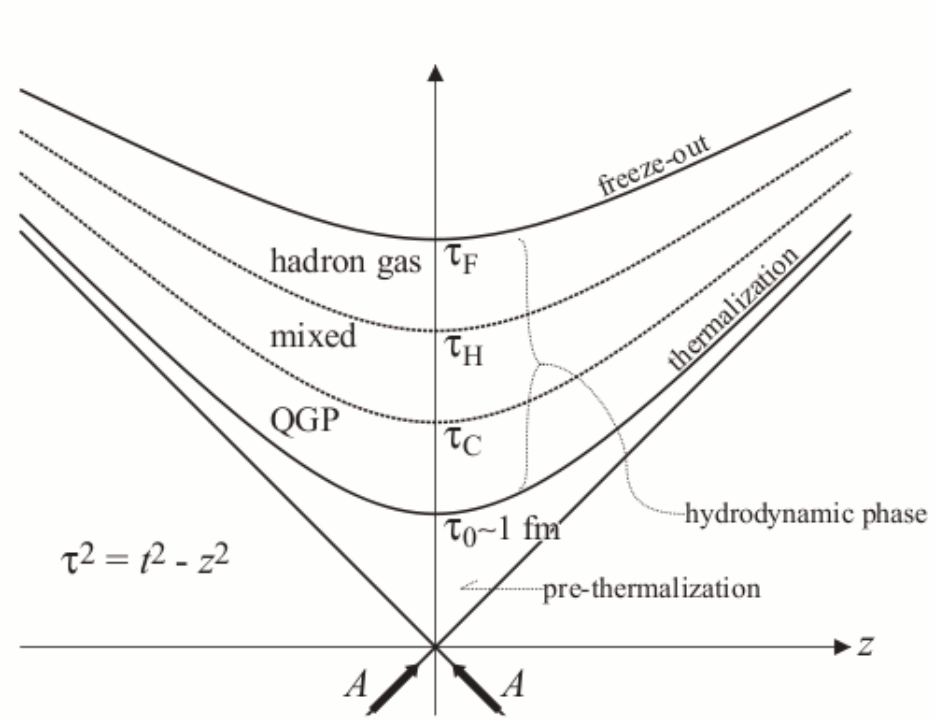

Figure 2: Space-Time Evolution of a Heavy Ion Collision, showing the proposed phase transitions throughout the evolution of the collision.

collision zone can vary from nearly circular to almond-shaped. The area and shape of overlap area (as well as number of participant nucleons) depends on the so-called impact parameter, b, which can be thought of as the vector in the transverse plane connecting the centers of the two nuclei. In the analysis the amount of overlap of the nuclei is generally expressed as "centrality", which is defined as the overlap area fraction (0% for fully central collision, 100% for the impact parameter equal to twice the radius of a nucleus). The impact parameter b and the beam axis z form the so-called "reaction plane", which defines the orientation of the two nuclei in space. As we can see in Fig.3, in a non-central collision the overlap area would have an almond shape, producing a spatially anisotropic chunk of matter. Then, the pressure gradients in the plasma drive the expansion in such a way that would convert this spacial anisotropy into a momentum anisotropy in the process more commonly known as

"flow". Investigations of the flow might hint at such properties of the plasma as pressure, viscosity, speed of sound, etc. as well as telling us whether the created medium is hadronic or quark-gluon. The theoretical predictions say that the hadronic medium would have high interaction length, therefore, having little inter-particle interactions and small flow, while a QGP medium is predicted to have small interaction length, causing the produced particles to undergo a large number of re-scattering before leaving the medium, leading to development of large pressure-driven hydrodynamic collective flow. Also, as the spatial anisotropy is the largest in the beginning of collision and quickly diminishes as the medium expands, the flow can be considered a good and useful probe of the early stage of collision.

2 Instrumentation

2.1 Relativistic Heavy Ion Collider

In order to produce energies required to obtain QGP, heavy ions have to be accelerated to extreme relativistic velocities. The earlier machines attempting to create such conditions were the Alternating Gradient Synchrotron (AGS) at Brookhaven National Laboratory and Super Proton Synchrotron (SPS) at CERN, with $\sqrt{s_{NN}}$ ranging from 4.8 to 19.4 GeV per nucleon for various ion species. The current experiment which provided the experimental data for this analisys is the Relativistic Heavy Ion Collider (RHIC). The Figure 4 shows the scematic drawing of RHIC structure. RHIC is a high-energy accelerator located in Brookhaven National Laboratory. RHIC is capable of accelerating and subsequently colliding beams of various particle species (p, d, several heavy-ion species), with center-of-mass energies of collisions up to 200 GeV per nucleon for Au nuclei. The acceleration of ions happens in several steps, with the beam going through several stages featuring smaller accelerators be-

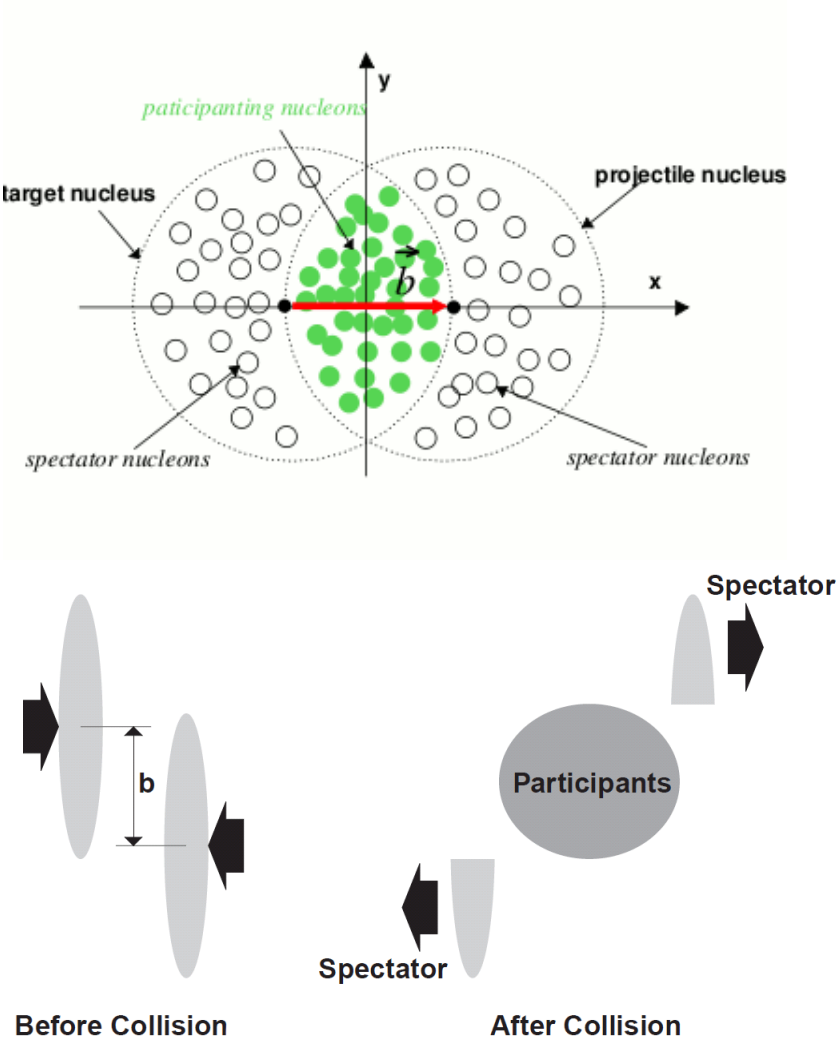

Figure 3: Geometry of a non-central collison, transverse plane view on the top, side view on the bottom

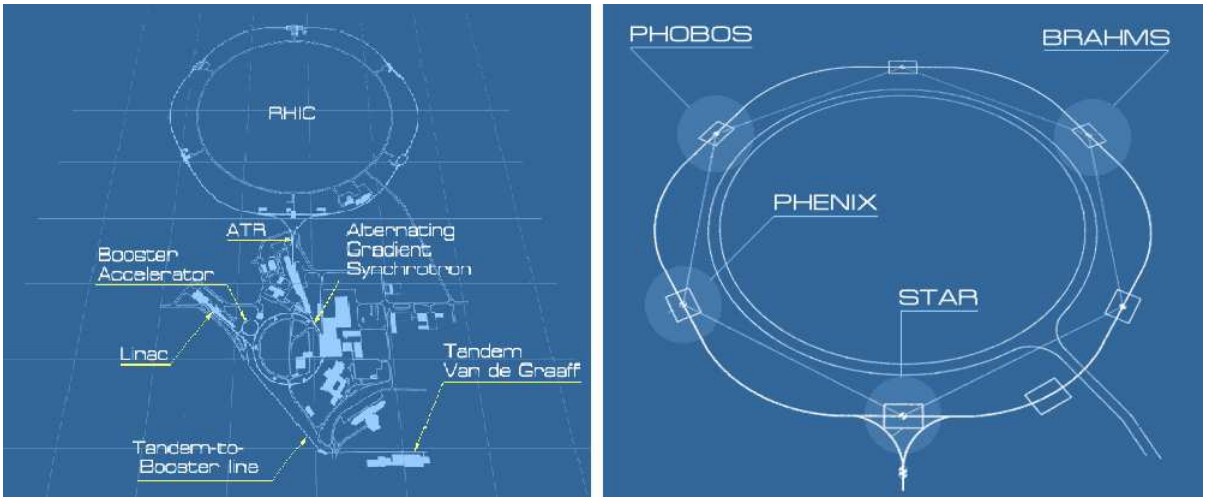

Figure 4: Relativistic Heavy Ion Collider

fore being injected into the storage rings. RHIC is one of the most powerful instruments for heavy ion collisions in the world, rivaled only by the CERN'S Large Hadronic Collider with its proposed center of mass energy of 5 TeV per nucleon for Pb ions. RHIC drives two beams of Au ions in the opposite directions through a circular tunnel, with 6 intersection points where the collisions occur. The two major experiments, STAR and PHENIX, that are currently functioning at RHIC are located at two of those intersection points. Each beam consists of 56 "bunches", each bunch containing about 10^9 ions.

2.2 PHENIX Detector

PHENIX (Pioneering High Energy Nuclear Interaction Experiment) is one of the two currently running major experiments at RHIC. The primary goal of PHENIX is discovery and studies of QGP. PHENIX detector subsystems allow for measurement of leptonic, hadronic and photonic products of the collision, as well as providing good resolution global event measurements, such as event plane, centrality and such.

PHENIX is a very complex instrument, composed of a large number of detector subsystems. Figure 5 shows the layout of PHENIX, with the subsystems labeled. The detectors

that were actually used in this work are: the Zero-Degree Calorimeter, the Beam-to-Beam Counter, the Reaction Plane Detector (global) , the Drift Chamber, the Pad Chambers, the Time-Of-Flight and the Electromagnetic Calorimeter (central arm, tracking). The global detectors measure the variables related to the whole event, such as centrality, event plane angle, multiplicity and the vertex location, while the central arm detectors (located at a pseudorapidity range of -0.35 to 0.35) allow for tracking individual particles and obtaining such information as particle's momentum, spatial location and direction of a track and providing information about the particle's identity. The PHENIX magnet system provides a magnetic field parallel to the beam in an area from the beam pipe to the Drift Chamber, making the charged particle tracks bend in the transverse plane, and therefore allowing the measurement of charged particle momentum.

2.2.1 Zero-Degree Calorimeter

The Zero-Degree Calorimeter (ZDC) is a pair of small hadron calorimeters made of layers of tungsten absorbers and scintillator. ZDC is located up and down along the beam axis about 20 meters from the interaction point. The purpose of ZDC is to detect the neutrons produced in the process of fragmentation of the remainders of the two nuclei after the collision (the charged particles are swept away by the magnetic field before they have a chance to reach the ZDC). That information is used to provide the estimate of the collision's centrality. Another purpose of this detector is to provide the event trigger.

2.2.2 Beam-to-beam Counter

The Beam-to-Beam Counter (BBC) is a set of two detectors positioned at forward and backward rapidities ($3.0 < |\eta| < 3.9$), at 144 cm from the interaction point. The Beam-to-Beam

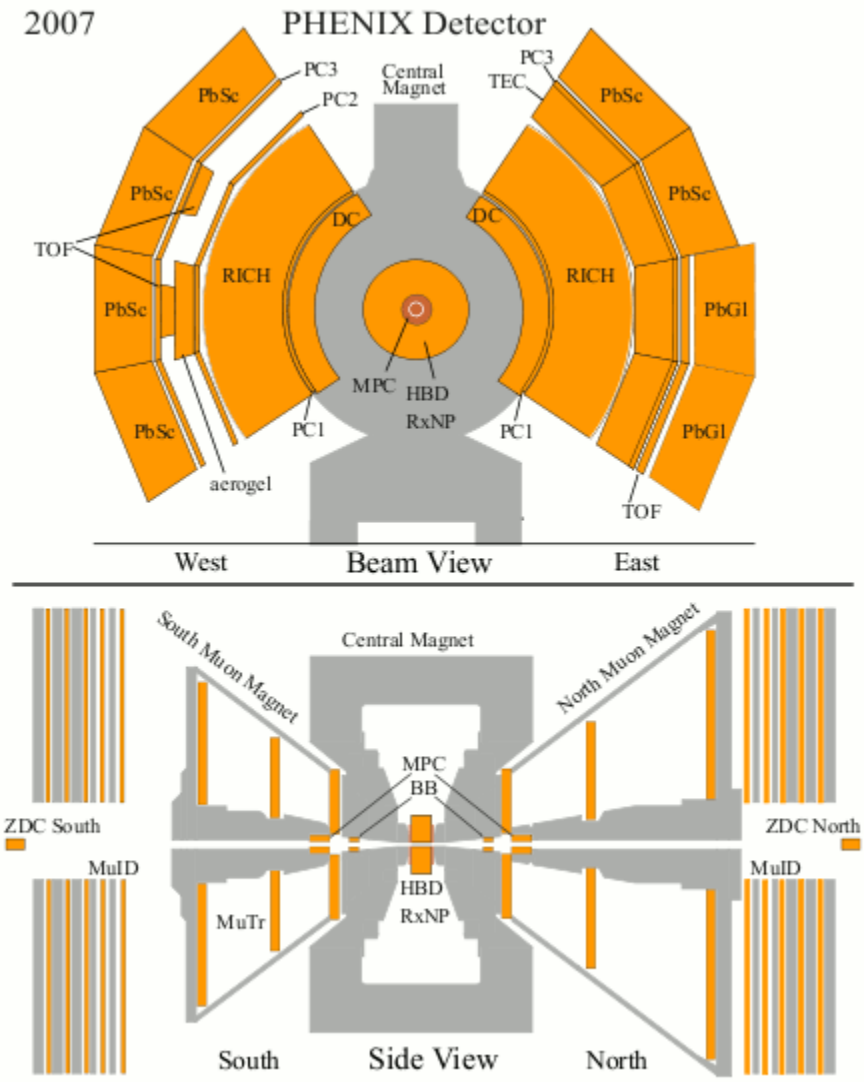

Figure 5: PHENIX Detector Layout

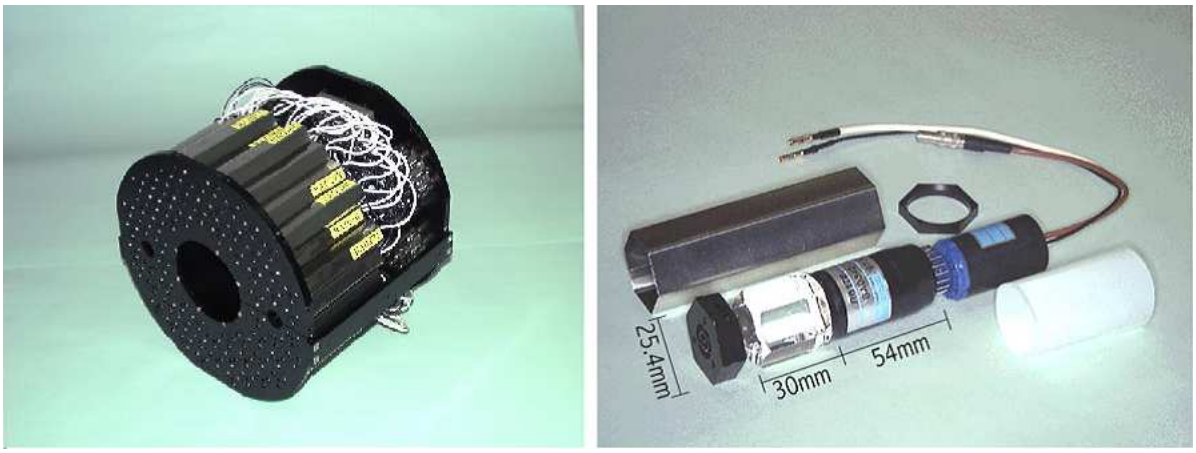

Figure 6: The Beam-To-Beam Counter. Left - the entire BBC; right - a single BBC element.

counter plays an important role in measuring the collision's centrality, as well as providing information on collision vertex location and start time for time-of-flight measurements. Also, a coincidence in the two BBC's is required for the event trigger. BBC is composed of 64 elements that are located symmetricaly around the beam axis, therefore, allowing usage of the hit distribution in BBC for event plane angle measurements. Each BBC element consists of a quartz Cherenkov radiator with a PMT reading out the signal. Figure 6 shows the entire BBC detector and a single BBC element.

2.2.3 Reaction Plane Detector

The Reaction Plane Detector (RXN) is a relatively new (since RUN7) detector used for estimation of the reaction plane. It provides a significantly better resolution in the reaction plane measurements than BBC. The RXN detector covers a pseudo-rapidity range of 1 to 1.5 (inner ring); 1.5 to 2.8 (outer ring). RXN makes use of plastic scintillator and PMT's to detect the charged particles. Similarly to the two detectors described above, the RXN detector consists of South and North halves. Yet another benefit of RXN detector in determining the event plane (as compared to BBC) is its separation into Inner and Outer

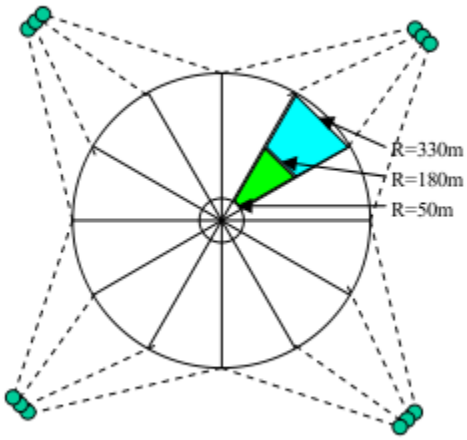

Figure 7: RXN detector layout

ring, which allows for more ways to determine the event plane resolution. The Figure Fig.7 illustrates the layout of RXN detector.

2.2.4 Drift Chamber

The Drift Chamber is the first tracking detector that the particles encounter. It is located in the central arms, 2 meters away from the beam axis, covering two 90 degree arcs in azimuth and 1.8 m in z direction ($|\eta| \leq 0.35$). The DC is situated within the magnetic field of the PHENIX magnet, which allows charged particle momentum measurements to be made. The angle of particle track as it leaves DC depends on the particle's momentum, allowing its determination.

2.2.5 Pad Chamber

The Pad Chamber (PC) is a tracking detector with three layers, located at 2.5, 4.2 and 4.9 m from the interaction point. Its purpose is to provide tracking by giving three-dimensional hit coordinates that can be correlated to each other to form a track through the detector.

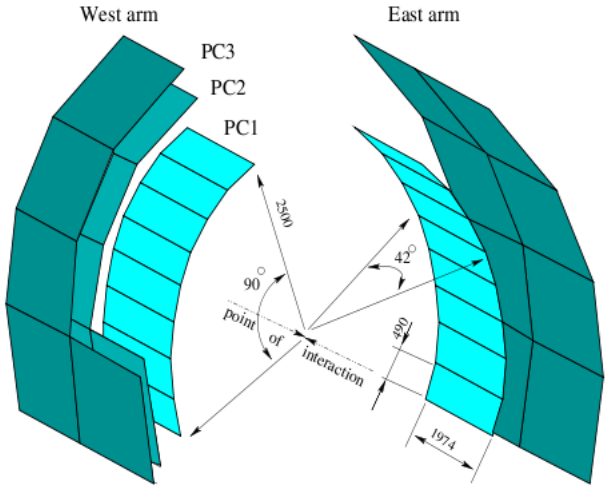

Figure 8: Pad Chamber geometry, showing the East and West arms and the three consecutive layers.

The PC is a multi-wire proportional chamber with a good position resolution (1.7, 3.1, 3.6 mm for PC1, 2 and 3). PC1 serves to start tracking the particle after it exits the DC and PC3 is positioned before the Electro-Magnetic Calorimeter. As well as the DC, the Pad Chamber covers two 90 degree arcs in azimuth. Fig.8 illustrates the Pad Chambers' layout.

2.2.6 Time Of Flight

The Time-Of-Flight (TOF) detector is yet another central arm detector that can be used for tracking, however, its main purpose is charged hadron identification. TOF has an excelent timing resolution which, when combined with our knowledge of a particle's momentum allows for calculating the particle's mass. TOF is located 5.05 meters away from the vertex and has timing resolution of 100 ps which means TOF allows for differentiating between pions and kaons with momentums up to 2.5 GeV/c and kaons and protons up to 4 GeV/c.

3 Event and Track Selection

This section summarizes the data selection and quality assurance procedures done in order to make sure the results are valid and meaningful. The data used in this analysis had been taken from PHENIX Run7 (year 2007), Au+Au collisions with $\sqrt{s_{NN}} = 200$GeV.

During the run, data collected by each one of the PHENIX detectors is taken and stored in a database. Afterwards, there are established calibration procedures that are done in order to make sure the data reflects the real picture. In order to ensure the quality of data is good, a number of checks have to be made, including checks on the quality of centrality and reaction plane measurements and track matching that reduces the background for the particle tracking.

3.1 Run QA and selection

A number of checks were performed to assure the quality of measurements such as event plane and centrality. During the experiment, collisions occur with random impact parameter and reaction plane orientation, distributed with equal probability. Consequently, the measured distributions of these variables should be flat. Improper calibration or detector misfunction may cause deviations from this behavior, which can be checked for. Each run's centrality distribution was fit with a line, and the χ^2/ndf calculated for the fits, allowing to check the degree of deviation from flatness. The Fig.9 shows the χ^2/ndf and mean values for the centrality distribution (on the top) and mean and width values for the Z vertex distribution fit with a Gaussian. Similarly, for event plane, the distibution was fit with a Fourier function. The coefficients obtained from the fit can be used to quantify the deviation. In case of large deviations observed, there is a flattening procedure established in calibration methods used by PHENIX that is employed to make the distribution flat. In order to make sure the

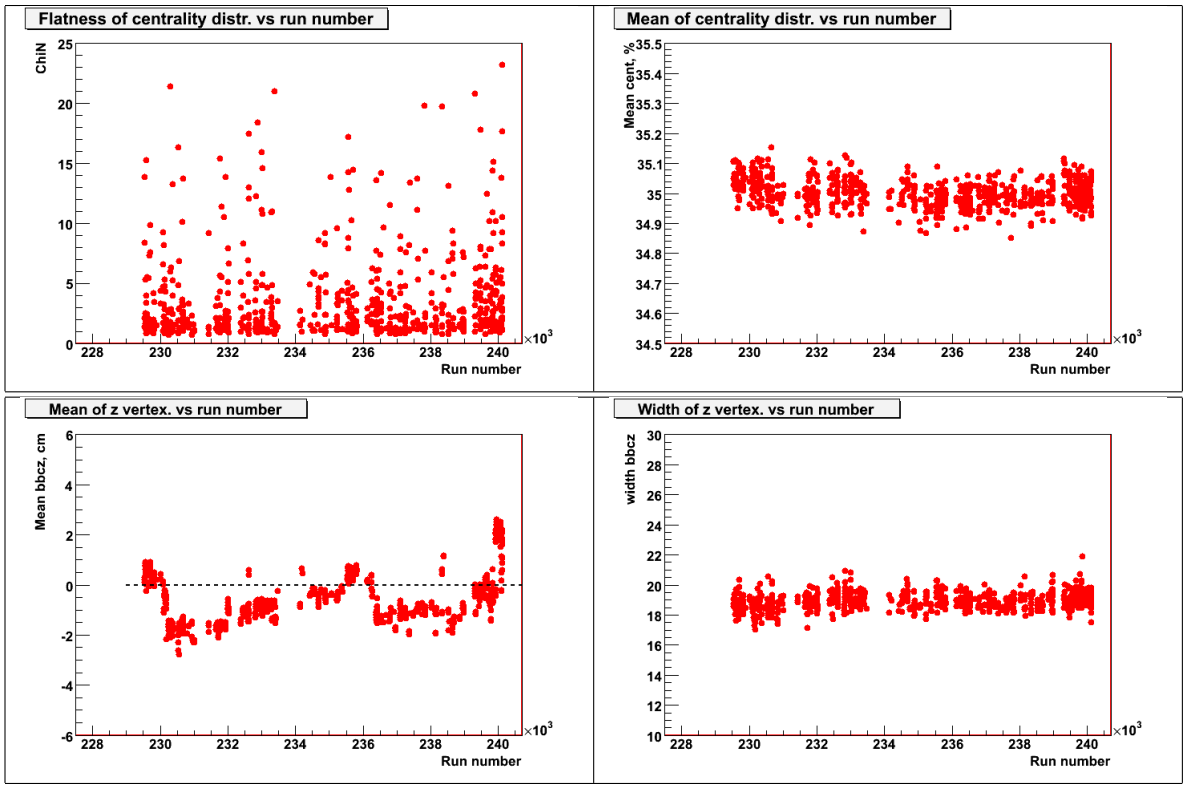

Figure 9: Centrality χ^2/ndf and mean; BBC Z vertex coordinate mean and width

event plane calibration is done properly, the flatness check needs to be done for both North and South halves of a detector and for the combined reaction plane. The Fig.10, Fig.11 and Fig.12 show the degree of flatness of the North, South and combined RXN plane respectively for each of the centrality bins, plotted against the run number. As those figures show, the deviations from flatness are relatively minor, with the second coefficient of the Fourier fit being below 0.002.

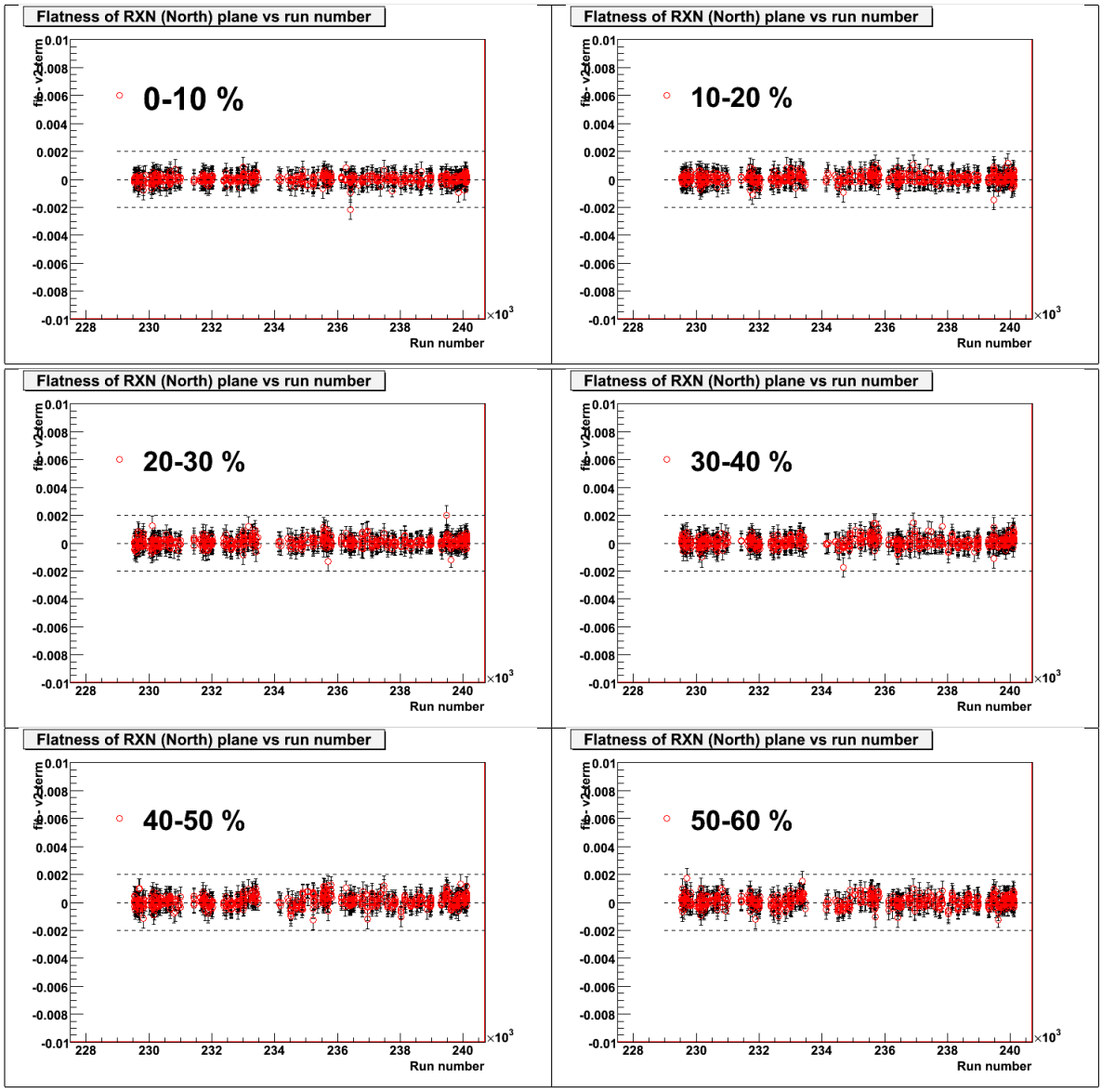

Figure 10: Event plane flatness for RXN North

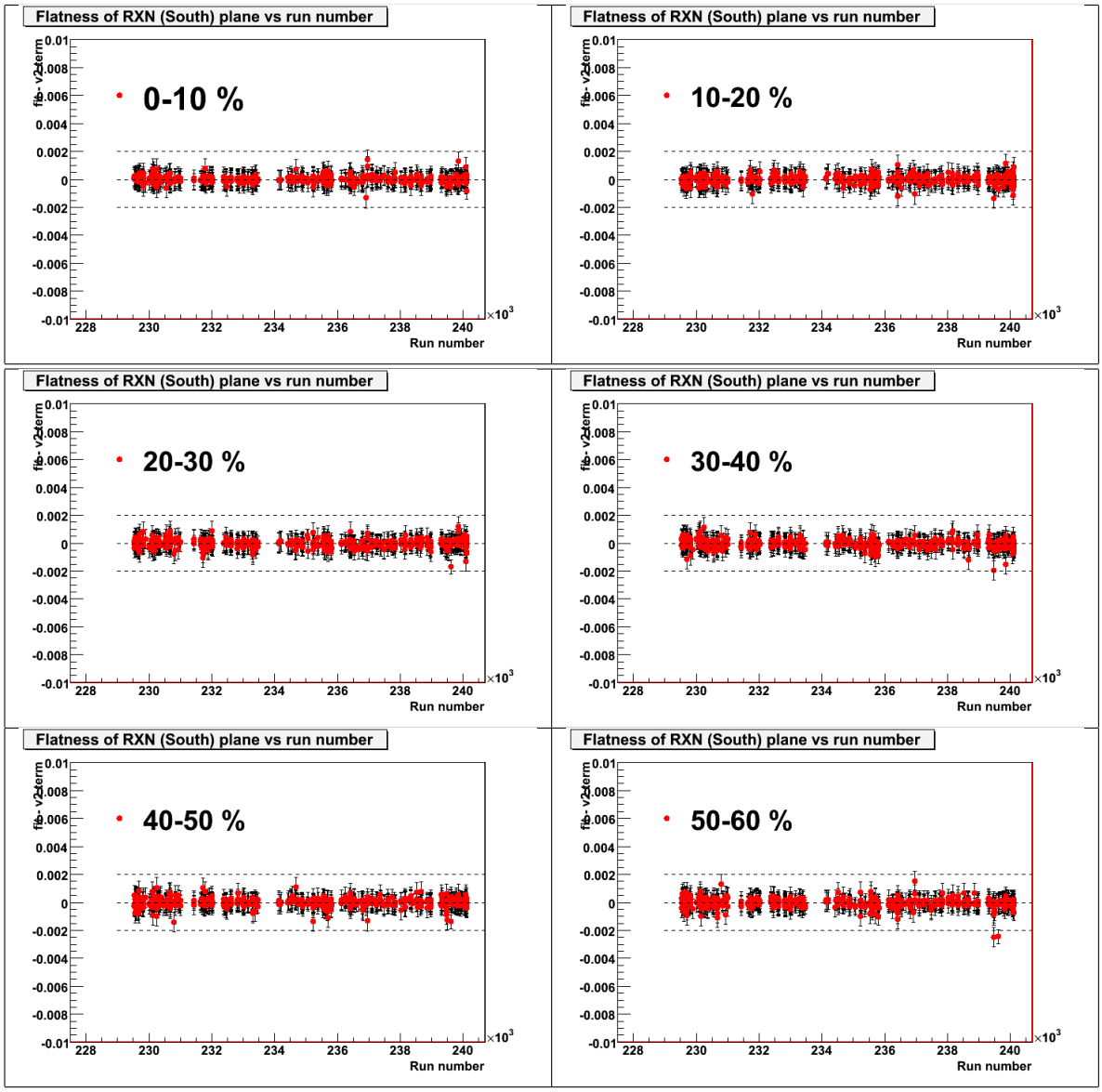

Figure 11: Event plane flatness for RXN South

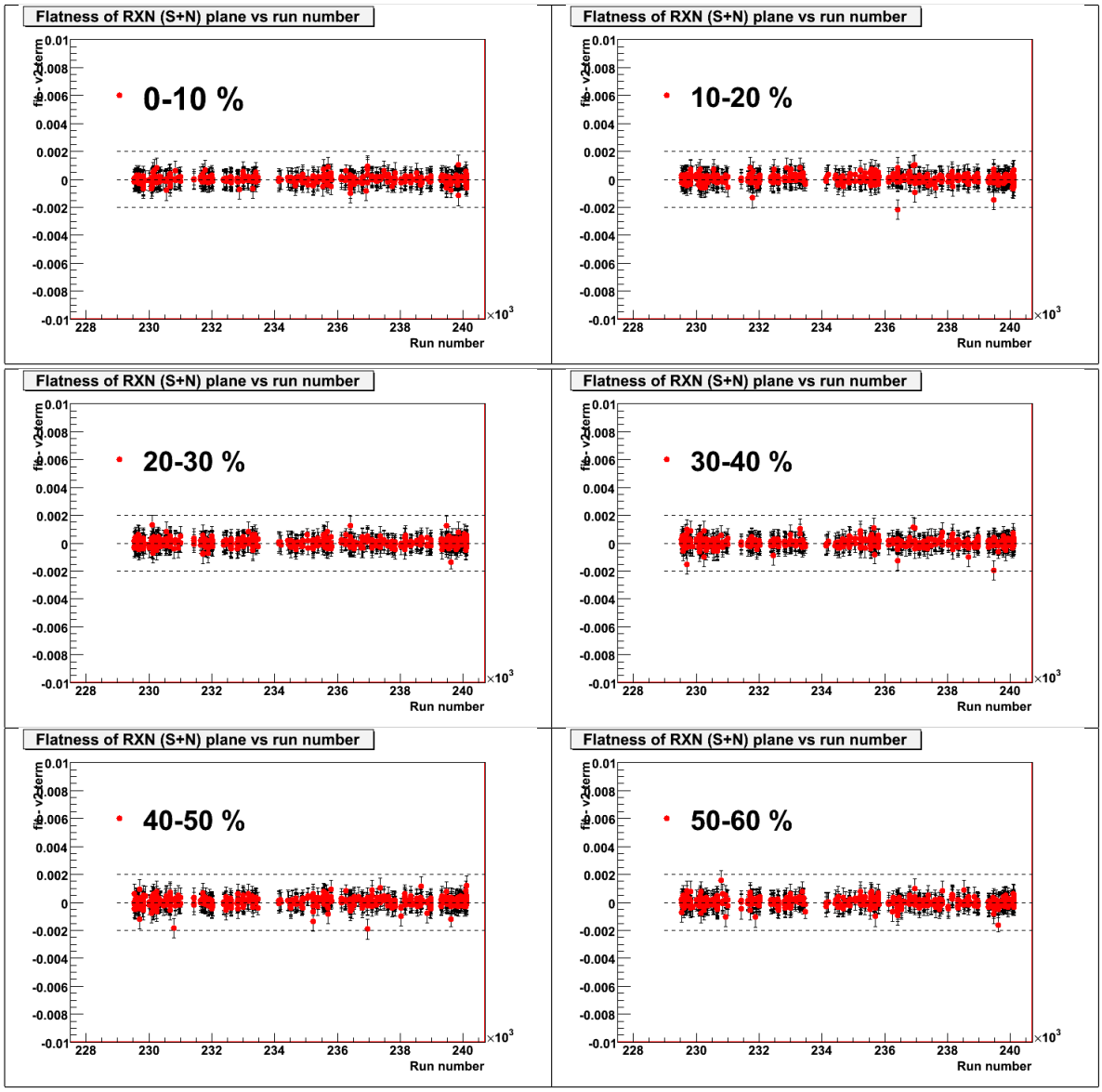

Figure 12: Event plane flatness for RXN South+North combined

3.2 Event Selection

In this analysis, $\sqrt{s_{NN}}$=200 GeV Au+Au data from RHIC Run 2007 was used. About 3 billion events were collected by PHENIX during Run 7. The minimum bias for events required a coincidence in both South and North halves of the BBC, as well as South and North ZDC. The vertex z coordinate as measured by BBC was required to be within ±30 cm. Out of the total bulk of events, 0-50% centrality events (central to mid-central) were selected and used for analysis.

3.3 Track reconstruction, selection and matching

The first tracking detector a charged particle hits on its way out is the Drift Chamber (DC). The DC is used to provide two important pieces of data: the particle's momentum and the starting point for tracking. While the Drift Chamber can identify particle momentum with good resolution (for primary particles coming from the collision vertex), a large amount of background still exists due to particle decays which can occur before the particle reaches the DC. Considering that the particle's momentum is determined by the angle of bend in DC's magnetic field, a low momentum particle (charged or neutral) that decays near DC can have a secondary vertex quite far from the primary vertex used for momentum determination. Therefore, the tracks for such decay particles could be misreconstructed as a high-momentum particle. As the number of low-momentum particles produced is much larger than the number of real high-momentum particles (the p spectrum is approximately exponential), the number of such misidentified particles can easily swamp the high momentum range. As the high momentum particle tracks are rather straight, matching the particle's hits on outer detectors (Pad Chamber, Time Of Flight, Electro-Magnetic Calorimeter) with a projected track location can allow us to eliminate some of that background. The low-energy particles

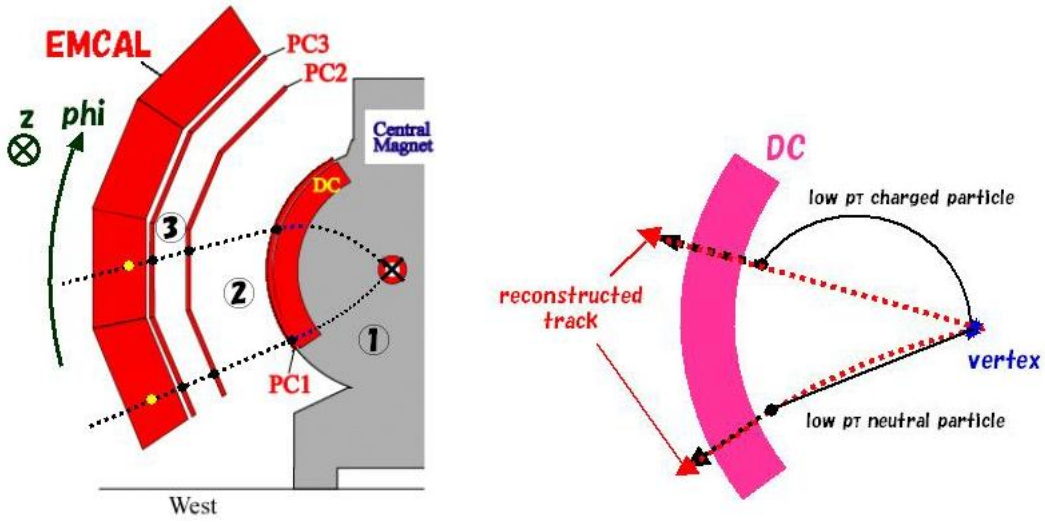

Figure 13: Illustration for track mathing (left), decay background (right)

that are mistaken for a high-energy ones are more influenced by the residual magnetic field and multiple scattering, therefore, having a higher probability to have larger deviations from the track predicted by track model. The Fig.13 illustrates the track model (on the left) and the decay background (on the right).

In order to understand the particle's path past the Drift Chamber and Pad Chamber 1, a particle's track needs to be reconstructed with regards to the hits on outer detectors. Each of those detectors can be thought of as a two-dimentional wall at a certain radius from the interaction region, providing us the three-dimentional coordinates for the hit. The track model provides a theoretical hit location, allowing an area around it to be searched for the closest actual hit. The hit coordinates are usually stored separately in terms of the z coordinate and the phi angle. Figure 14 shows a typical hit distributions before the cuts are made.

The distance between the projected and the actual hit location in z and phi coordinates follows an approximately Gaussian distribution which we can fit with a Gaussian function. The width provided by the fit can be used to store the distance of the hit in z and phi from

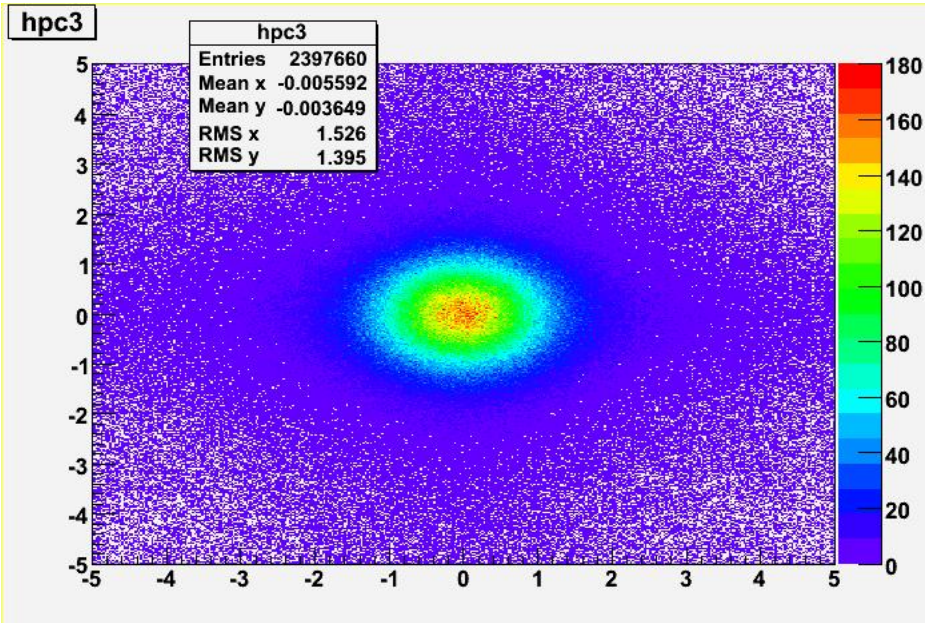

Figure 14: $dz/d\phi$ distribution on PC3. The axis are dz and dϕ values for hit locations, normalized by a Gaussian fit.

the projected location in terms of standard deviation. The mean and the width can be also used to check the integrity of our tracking by looking at these variables as a function of event centrality, momentum, z and phi of the track, charge of the particle etc. In case if the resulting distributions show strong dependence on those variables, futher corrections are applied.

4 Flow Analysis

Azimuthal anisotropy is known to be a sensitive probe of the transport properties of the QGP [7]. Therefore, investigation of elliptic flow is important for understanding what happens in heavy ion collisions. In this section, the methods for elliptic flow analysis are described.

4.1 Reaction plane determination

In order to measure the flow, the event plane angle must be measured first. The detectors that can be used in the event plane determination are RXN and BBC. Those detectors are symmetrical around the beam axis and allow the event plane to be measured using the anisotropy itself. The distribution of particle hits between the sectors of the detector can give us the event flow vector Q:

$Q_x = Q_n \cos(n\Psi_n) = \sum_i^M w_i \cos(n\phi_i)$

$Q_y = Q_n \sin(n\Psi_n) = \sum_i^M w_i \sin(n\phi_i)$

$\Psi_n = \frac{1}{n} \arctan\left(\frac{Q_y}{Q_x}\right)$,

where M is the number of particles, n is the humber of the harmonic (2 for the elliptic flow), w is weighting factor used to optimize reaction plane resolution. (if kept to 1, then the reaction plane is calculated in a way that is determined by the number of particles hitting the detector at various angles) and ϕ is the asimuthal angle of the particle.

4.2 v_2 extraction

As the azimuthal distribution is a function of the azimuthal angle, it is natural to write it out in the form of Fourier expansion. We use the second Fourier harmonic (v_2) as it corresponds to the elliptic flow, which is the major phenomenon studied in this analysis.

$\frac{dN}{d\phi} = N_0(1 + \sum_i 2v_2 \cos[2(\phi_i - \Psi_{RP})]$,

where N_0 is the normalization constant, v_2 is the coefficient that shows the magnitude of anisotropy, $\frac{dN}{d\phi}$ is the azimuthal distribution of the particles, Ψ_{RP} is the event plane orientation in the detector coordinate system and ϕ_i is the angle of each particle track in the detector coordinate system. The summation is done over all of the events in a given bin. In the analysis, every particle in each event is correlated to this event's reaction plane,

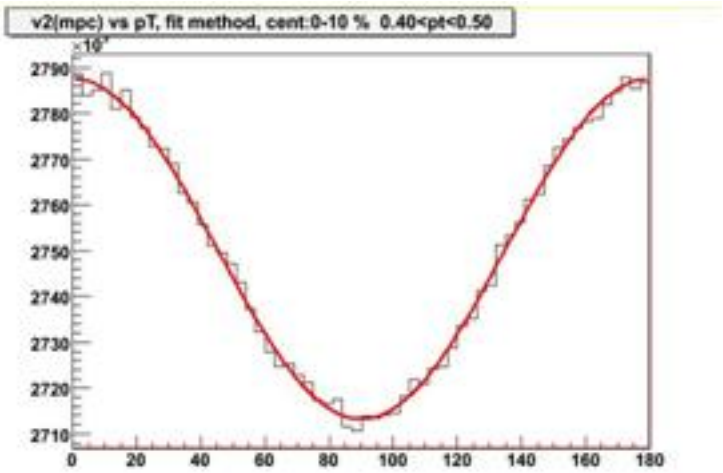

Figure 15: Asimuthal distribution of the particles with a Fourier fit

giving us the angle $(\phi - \Psi_{RP})$, which is the angle of the particle relative to the event plane. The Fourier analysis of the azimuthal distribution gives us

$$v_2 = < \cos(2(\phi - \Psi_2)) >, \tag{1}$$

where Ψ_2 is the event plane angle, ϕ is the azimuthal angle of each particle and the average is taken over all the particles over all of the events in a given centrality and transverse momentum bin. Also, the azimuthal distribution of the particles can be fit with a $N_0(1 + 2v_2 \cos(2(\phi - \Psi_2)))$ function, which gives essentially the same results. Figure 15 shows an example particle distribution (for 0-10% centrality and $0.4 < p_T < 0.5$GeV) fitted with such a fit.

4.3 Event Plane Resolution

The measured event plane angle Ψ_2 that is obtained from the detector is only an approximation for the true reaction plane Ψ_{rp}. Therefore, the raw v_2 values obtained by the method described in the previous section are lower than the true v_2 values and must be corrected

with regard to this error. Knowing the event plane resolution, we can find a correction coefficient σ, such that $v_2 = v_2^{obs}/\sigma$. In this section, methods for evaluating the event plane resolution and correcting the v_2 results with regard to it are described.

The $[\Psi_2 - \Psi_{rp}]$ distribution is a function of a parameter χ_m which measures the reaction plane dispersion. χ_m is proportional to the flow signal and scales with the event multiplicity (N) as square root of it. The event plane resolution can be expressed through it as:

$$< \cos(n(\Psi_2 - \Psi_{rp})) >= \frac{\sqrt{\pi}}{2\sqrt{2}}\chi_m \exp(-\chi_m^2/4)\left[I_{\frac{k-1}{2}}(\chi_m^2/4) + I_{\frac{k+1}{2}}(\chi_m^2/4)\right] \quad (2)$$

where I_ν is the modied Bessel function of order ν.

4.3.1 2-Subevent Method

The reaction plane dispersion can be estimated by measuring the event plane angle in two independent sub-events of similar multiplicity, for example, South and North part of BBC or RXN detector. The resolution for one such subevent can be calculated using the formula

$$< \cos(n(\Psi_n^a - \Psi_{rp})) >= \sqrt{< \cos(n(\Psi_n^a - \Psi_n^b)) >} \quad (3)$$

, where Ψ_n^a and Ψ_n^b are the two subevent event planes.

Knowing that χ_m scales with multiplicity as $\sqrt{N}$, we can then extract the value of χ for the half-event using eq.(2) and use it to calculate χ_m and the resolution for the whole event. The value of χ can be also determined by fitting the distribution of the azimuthal difference between the two sub-event planes with a function

$\frac{e^{-\chi^2}}{2}\left[\frac{2}{\pi}(1+\chi^2) + z\,(I_0(z) + L_0(z)) + \chi^2\,(I_1(z) + L_1(z))\right]$

where $z = \chi^2 \cos(\triangle\phi_R)$ and L_0 and L_1 are modified Struve functions. An example of

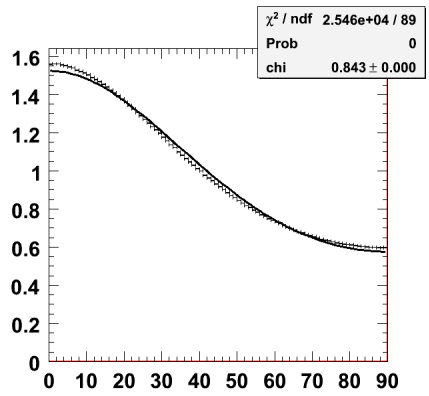

Figure 16: Reaction plane dispersion distribution for RXN detector.

the reaction plane dispersion distribution (RXN North - RXN South) fitted with the above function is given in Figure 16. The distribution in that figure has been taken from 30-40% centrality bin.

Figure 16 shows an example for the event plane dispersion. In this figure, we can see the distribution of the difference between the event planes measured by South and North half of the RXN detector, fitted with a function discussed above. It can be clearly seen on this figure that the resolution of the detector is fairly limited, therefore, requiring correction such as described above.

4.3.2 3-Subevent Method

One of the advantages of the PHENIX detector is the large number of subsystems that measure the reaction plane angle in several pseudo-rapidity windows. This allows for determination of resolution using three different sub-event planes to calculate the resolution. The main benefit of this method is being able to calculate the reaction plane resolution several times using several different sub-event sets, therefore, cross-checking the validity of the result.

$$< \cos(n(\Psi_n^a - \Psi_{rp})) >= \sqrt{\frac{< \cos(n(\Psi_n^a - \Psi_n^b)) >< \cos(n(\Psi_n^a - \Psi_n^c)) >}{< \cos(n(\Psi_n^b - \Psi_n^c)) >}} \quad (4)$$

where Ψ_n^a, Ψ_n^b and Ψ_n^c are the event planes from the three sub-events and Ψ_n is the true reaction plane.

The figure and tables below show the resolution correction factors calculated for the RXN and BBC detectors via variable methods. Figure 17 shows the difference in resolutions between the RXN and BBC detectors. We can clearly see that the RXN detector boasts a larger resolution (0.5 to 0.8) than the BBC (0.2 to 0.4). As was mentioned previously, the event plane resolution is expected to show dependency on two factors - event multiplicity and the strength of the flow signal. Resolutions shown here are consistent with such expectations - the highest resolution is seen at the mid-central region where both multiplicity and strength of the flow is fairly large and the lowest resolutions are seen at the central and periferal regions, where either strength of the flow or multiplicity is small. Figure 18 shows the difference between the two-subevent and three-subevent resolution coefficients, showing more or less good agreement for most of the centralities but the most central. RXN shows better agreement between those two methods than BBC.

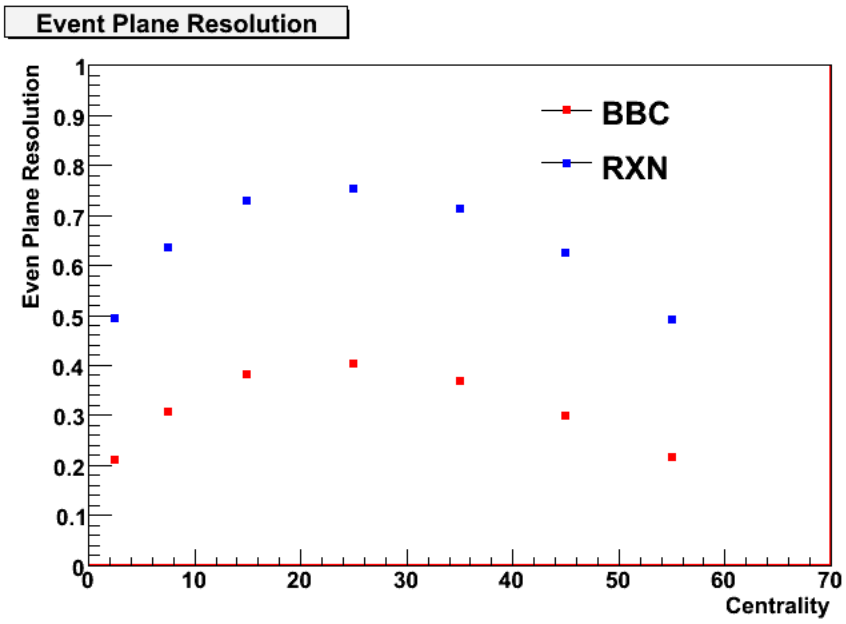

Figure 17: Event Plane Resolution correction factors for different centrality bins, for BBC and RXN detectors, calculated via 2-subevent Ollitrault fit method.

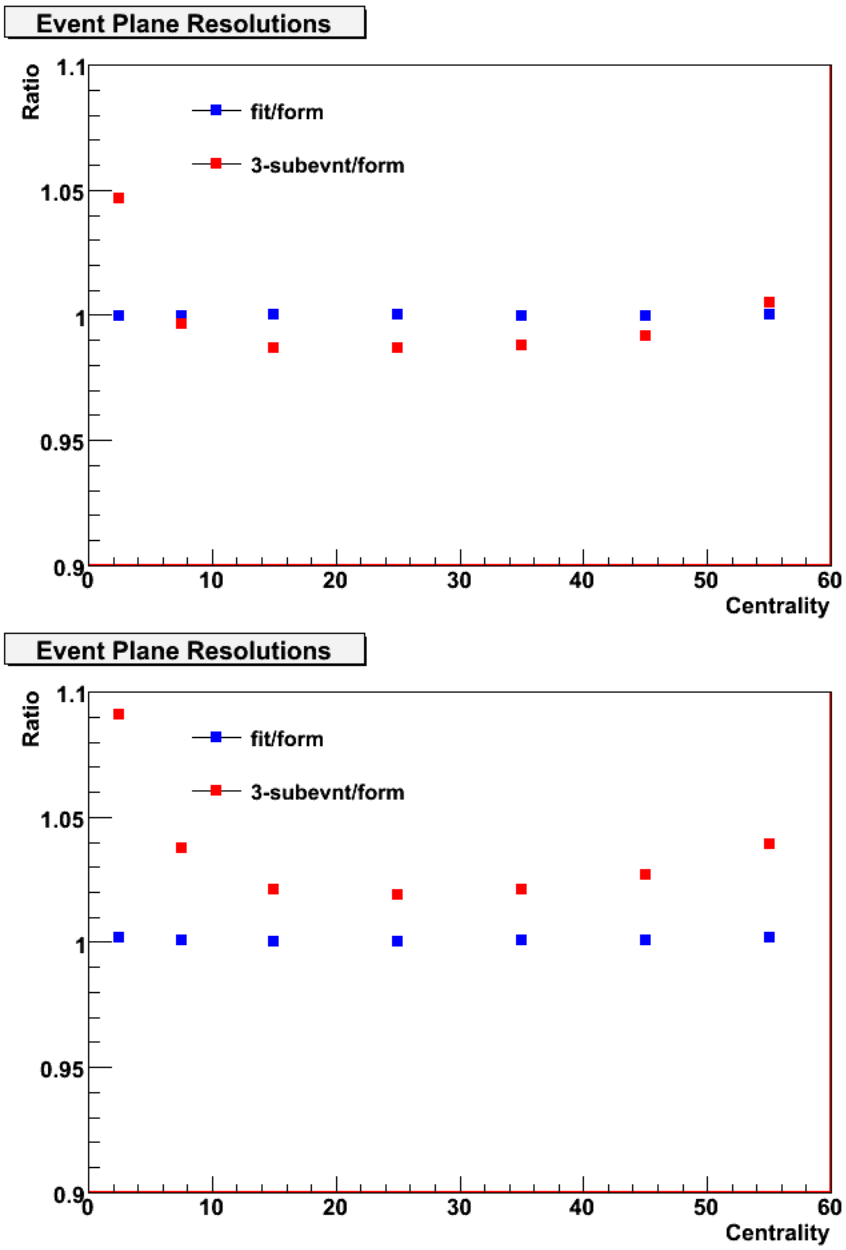

Figure 18: Event Plane resolution coefficients extracted by different methods (for RXN event plane on the top, for BBC on the bottom.

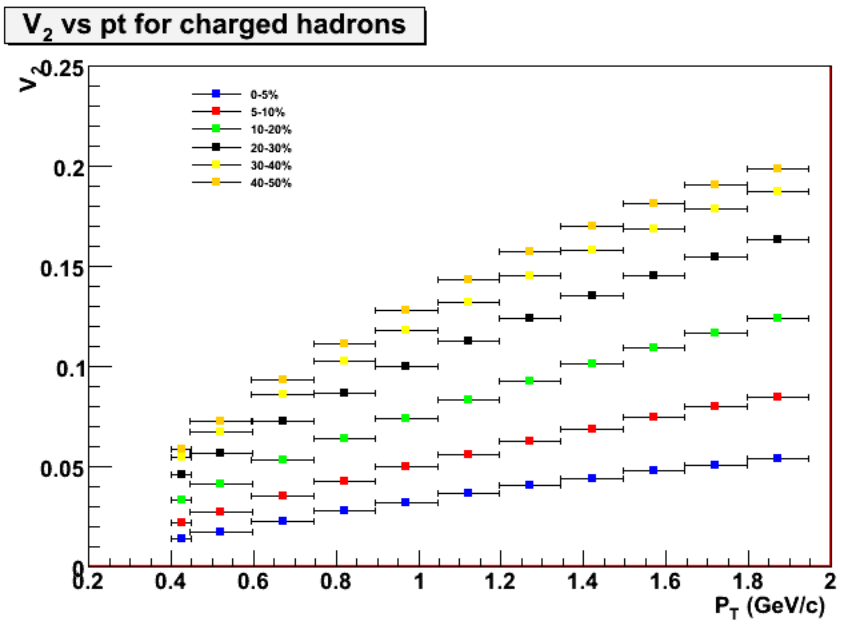

Figure 19: Charged hadron v_2 vs p_T for various centrality bins, calculated using RXN event plane. The bars represent the size of p_T bins

5 Results and discussion

In this section the results for the anisotropy measurement are reported. For this analysis, the PHENIX Run7 data of Au-Au collisions at 200 GeV were used. The events used are of centralities from 0 to 50, in the bins 0-5, 5-10 and then in 10% steps up to 50%. Values of v_2 are calculated for charged hadrons for p_T from 0.4 to 1.95 GeV/c. The v_2 dependence on transverse momentum and centrality of the collision was studied, as well as comparisons were made between the v_2 results calculated using different event planes. Comparison of the PHENIX results with the published results from the STAR experiment were also made.

5.1 PHENIX results

Fig. 19 shows the v_2 results produced using event plane method with respect to RXN event plane, corrected by two-subevent resolution method.

In this figure following dependencies can be observed:

v_2 dependence on centrality: Our understanding of heavy ion collisions is that depending on the geometry of a particular collision, the reaction zone can take different shapes. Depending on the impact parameter, the eccentricity of the collision zone can go from near zero at the most central collisions to high values in the mid-central ones and again decrease for very peripheral ones. As the hydrodynamic flow is thought to be controlled by the pressure gradients in the medium, the collision with higher eccentricity would produce larger flow. As can be seen from Fig. 19 (which covers the v_2 values for centrality bins from 0-5% (most central) to 40-50% (mid-central), the amount of observed flow increases with centrality, which is compatible with our understanding of the process of the collision.

$v_2$dependence on p_T: The hydrodynamic calculations predict the amount of flow that grows with the transverse momentum p_T. [7] At the p_T range that this analysis was done for, observed values of v_2 are seen to be proportional to the transverse momentum, again compatible with our expectations.

As PHENIX detector involves several subsystems that allow independent mea3urements of event plane, we can use the v_2 results calculated using those different event planes to cross-check our consistency. The figure Fig.20 demonstrates the ratios of v_2's measured by two different event planes (RXN and BBC). As we can see, the two measurements yield results that are consistently within less than 5% from each other and show little pt/centrality dependence.

The figure Fig.21 demonstrates the comparison of the results obtained in this analysis with previously published PHENIX results [3]. We can see that this analysis is consistent with the work previously done.

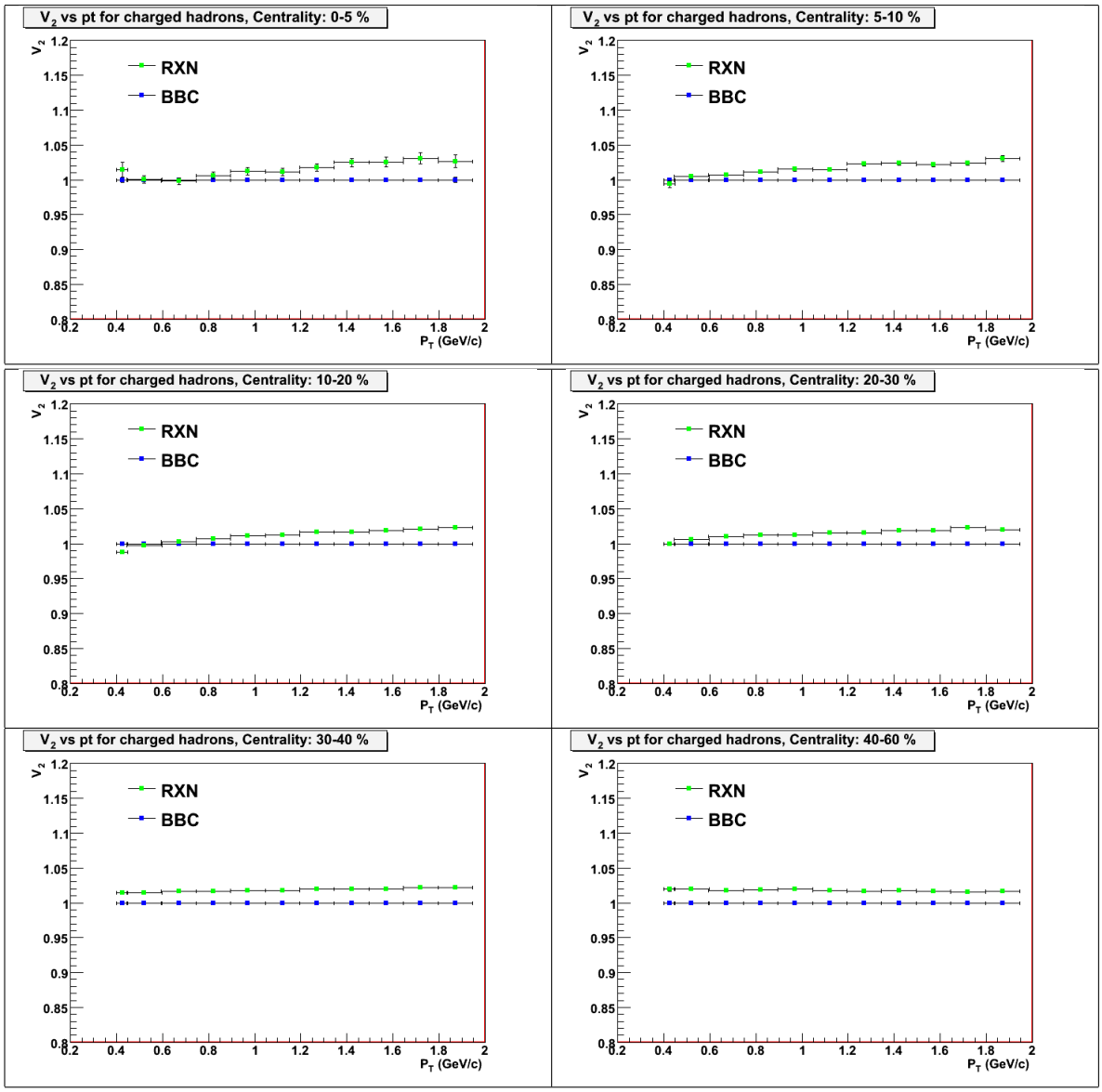

Figure 20: v_2 ratios RXN/BBC. The green points represent the ratio of v_2 measured with respect to RXN plane to v_2 with respect to BBC plane. The blue points are the baseline (RXN).

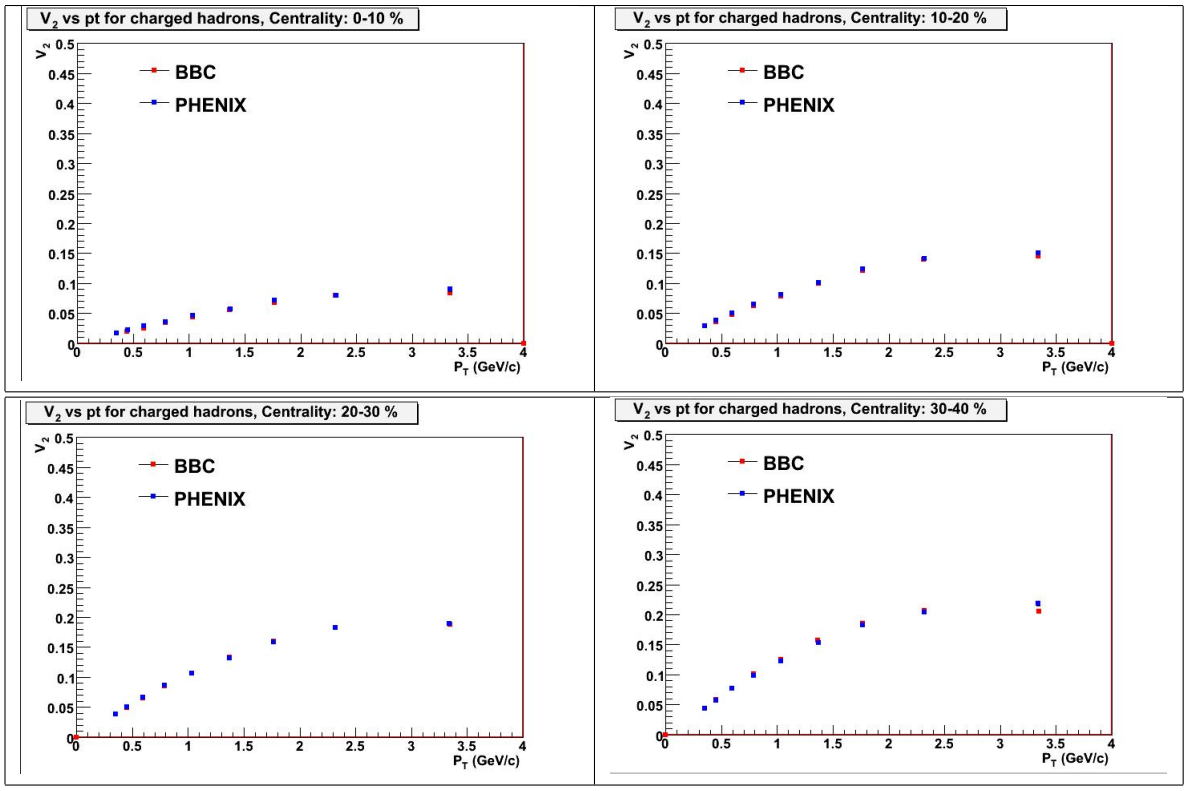

Figure 21: Comparison to previously published PHENIX Run7 data

5.2 STAR results

5.2.1 The STAR Detector.

As well as cross-checking measurements from separate event plane detectors, we can compare the PHENIX result with the results yielded by other experiments on RHIC. The Solenoid Tracker at RHIC (STAR) is the other big experiment currently running at RHIC. The STAR detector is also capable of producing data that can be analyzed to yield the measurements of particle production anisotropy. Comparing this independent measurement with the PHENIX results can give us further assurance of our results' integrity.

The STAR Detector is located at 6 o'clock position at RHIC. It consists of several subsystems covering full azimuth in the pseudorapidity range of $|\eta| < 1.8$ and $2.5 < |\eta| < 4.0$. The primary tracking device used by STAR is its Time Projection Chamber (TPC) at the

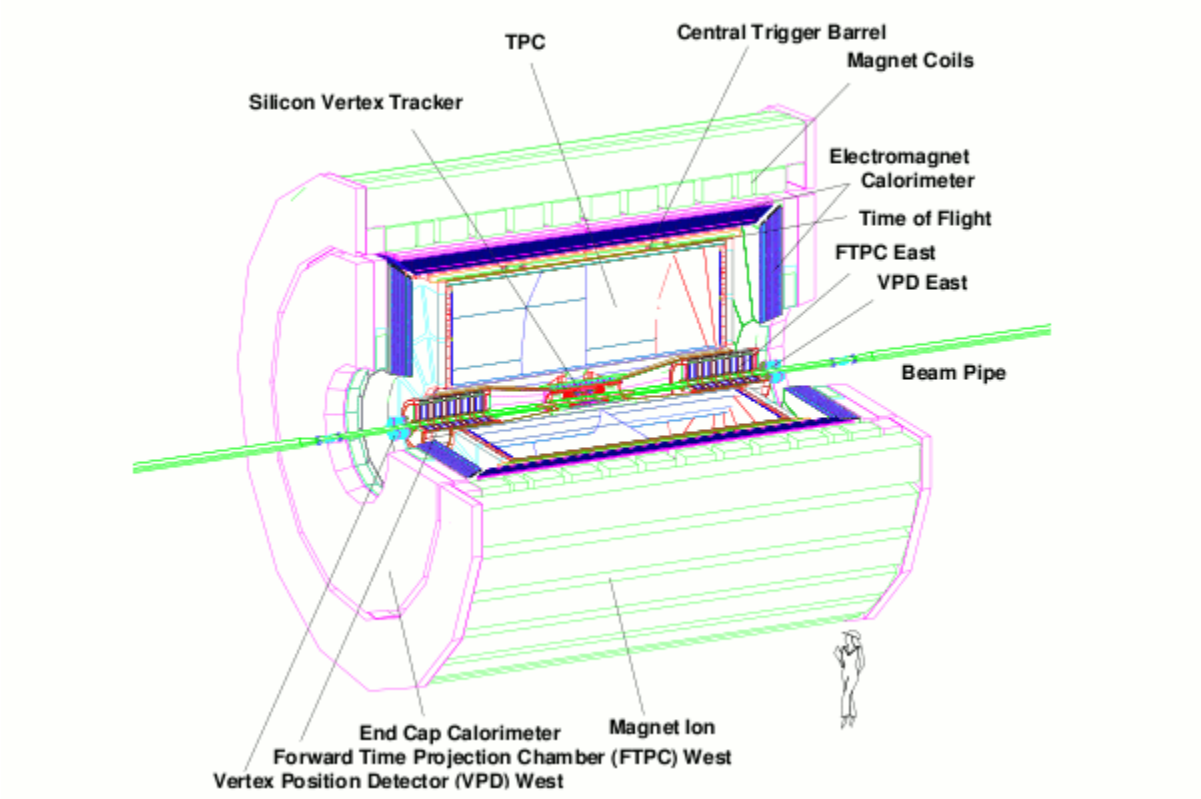

Figure 22: The STAR Detector

midrapidity and the Forward Time Projection Chambers at forward and backward rapidities.

5.2.2 STAR Results

The Fig. 23 shows the v_2 results published by the STAR collaboration in paper [8]. Those v_2 values have been calculated using the standard event plane method, corrected via 2-subevent resolution correction. The v_2 results from this publication show the same general p_T and centrality dependences as the PHENIX results discussed above. The analysis in this thesis has been done using similar binning in centrality and p_T with a goal to be able to compare the results.

5.2.3 PHENIX / STAR comparison

This figure shows the ratio of STAR published data to our current measurements.

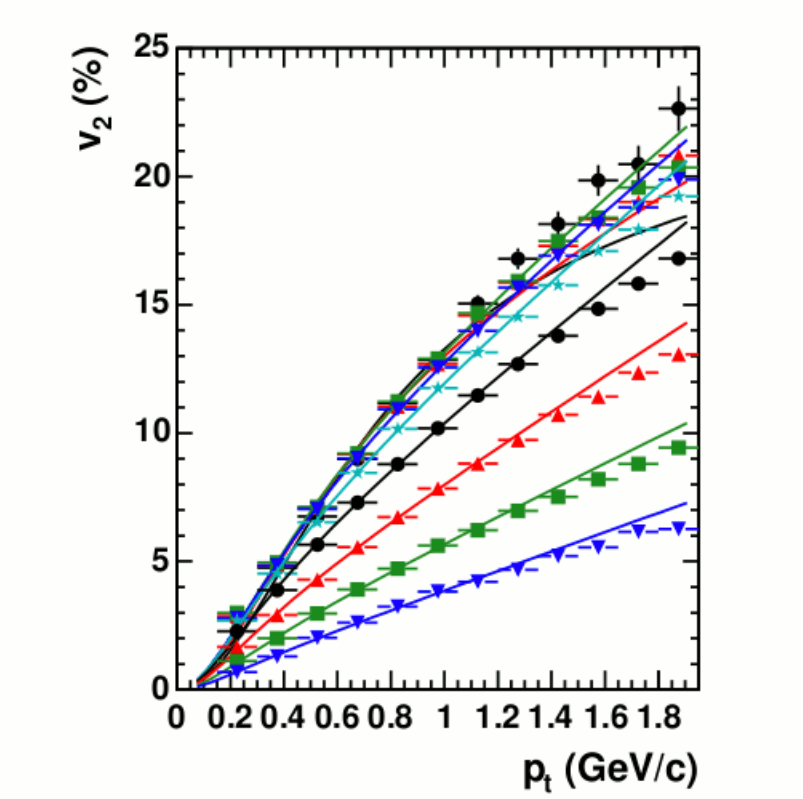

Figure 23: Charged hadron v_2 vs. p_T for the centrality bins (bottom to top) 5 to 10% and in steps of 10% starting at 10, 20, 30, 40, 50, 60, and 70 up to 80%. The solid lines are Blast Wave fits.

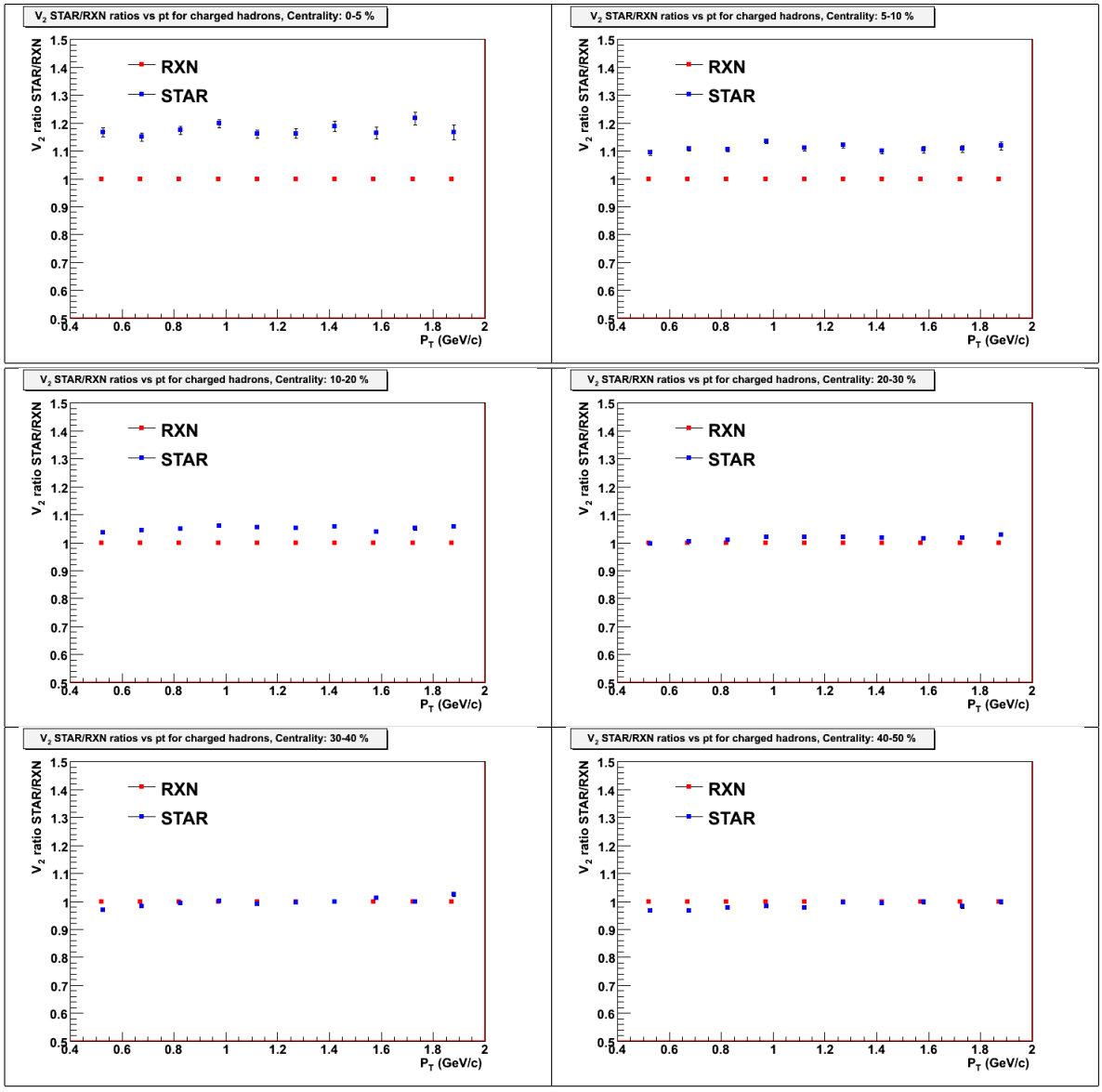

Figure 24: Ratios between v_2 values as measured by PHENIX and STAR. The blue points represent the ratio of v_2 measured by STAR to v_2 measured by PHENIX. The red points are the baseline (PHENIX)

The PHENIX v_2 results shown here were produced using the event plane method, using RXN as the event plane detector. The STAR results were produced using the even plane method as well, using the STAR TPC ($|\eta < 1|$) detector for both the event plane determination and particle tracking.

While comparing the measured v_2 values of STAR to PHENIX, we can see that the following trend. The differences between our results and STAR ones don't show any large pt-dependence, however, we can see the definite difference centrality-wise. The largest difference (STAR values being about 20% higher) is seen at 0-5% centrality bin, at 5-10% centrality the difference decreases to about 10%, while at the higher centralities the results shows consistency within 5%. One of the theories is the influence comes from non-flow effects, which could be higher in STAR due to the event plane measurement and track correlation to event plane being done in the same pseudorapidity range (the STAR central TPC). The rapidity gap between the tracking detector arm and the event plane detectors is thought to be reducing the non-flow correlations. The greatest difference being seen at the low centralities, where the v_2 is the lowest, seeming to be consistent with such explanation (if the non-flow effects don't depend that much on centrality).

Another possibility might be the difference in centrality definition between STAR and PHENIX. Such calibrations are done independently in different experiments, so it could be logical to assume that such differences could come from it. In order to check for such differences, v_2 values were calculated while "shifting" the centrality bins by some amount. That means that STAR's published values for 0-5% centrality bin were compared to calculated v_2 results from PHENIX for 0-6% and 0-7% centrality bins, STAR's 5-10% with 6-11% and 7-12% and so on. The effects of such shift were the following:

1) The difference between STAR and PHENIX results for the most central collision went

down considerably, for example, with 2% shift for 0-5% bin it decreased from about 20% to about 7%, for 5-10% it went down from 10% to below 5%.

2) For the less central collisions (bins 10-20% and above), the shift had a rather minor influence - the two results stayed within 5% from each other.

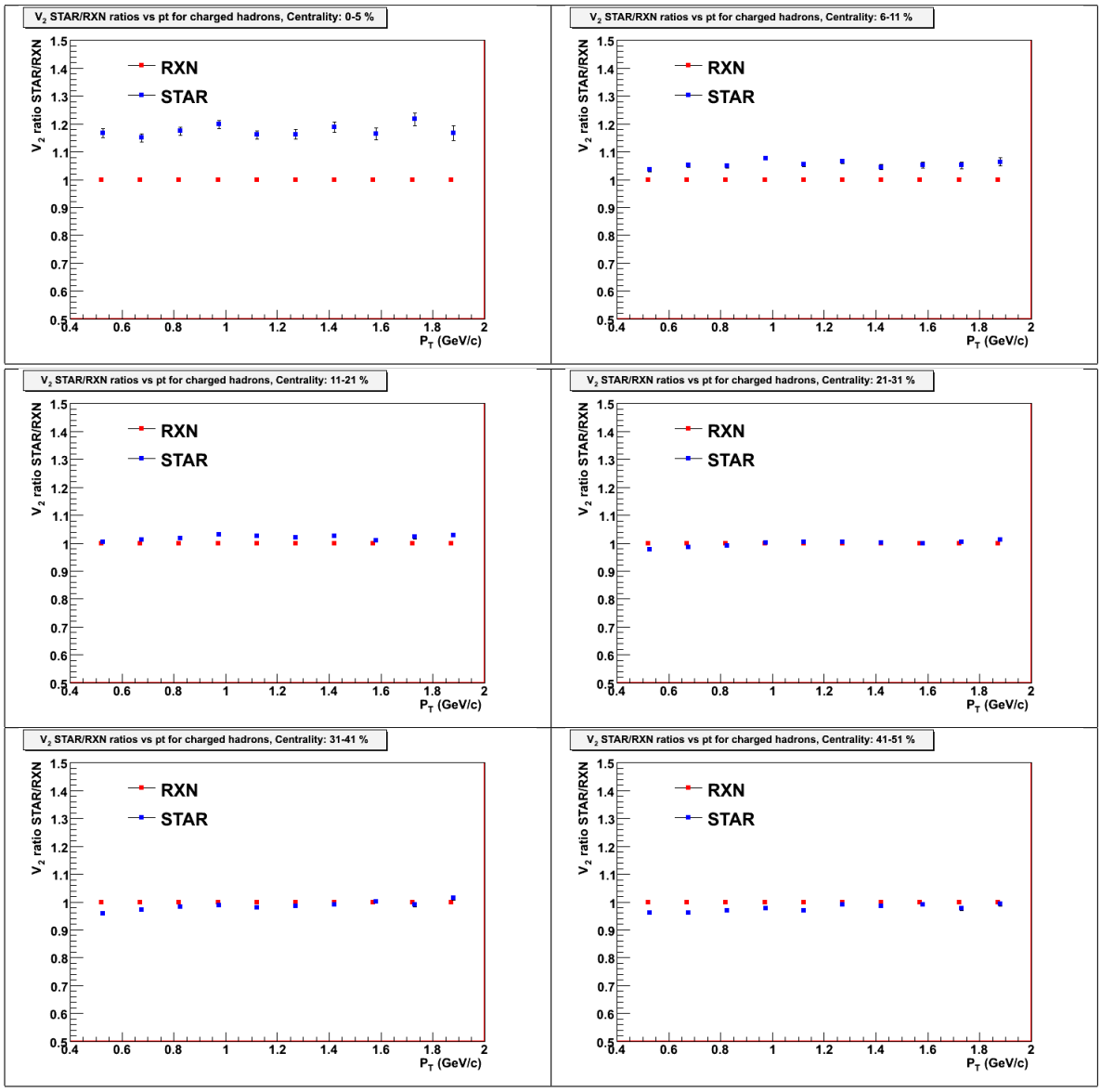

Figure 25: Same as Figure 24, but with 1% centrality shift (0-6-11-...)

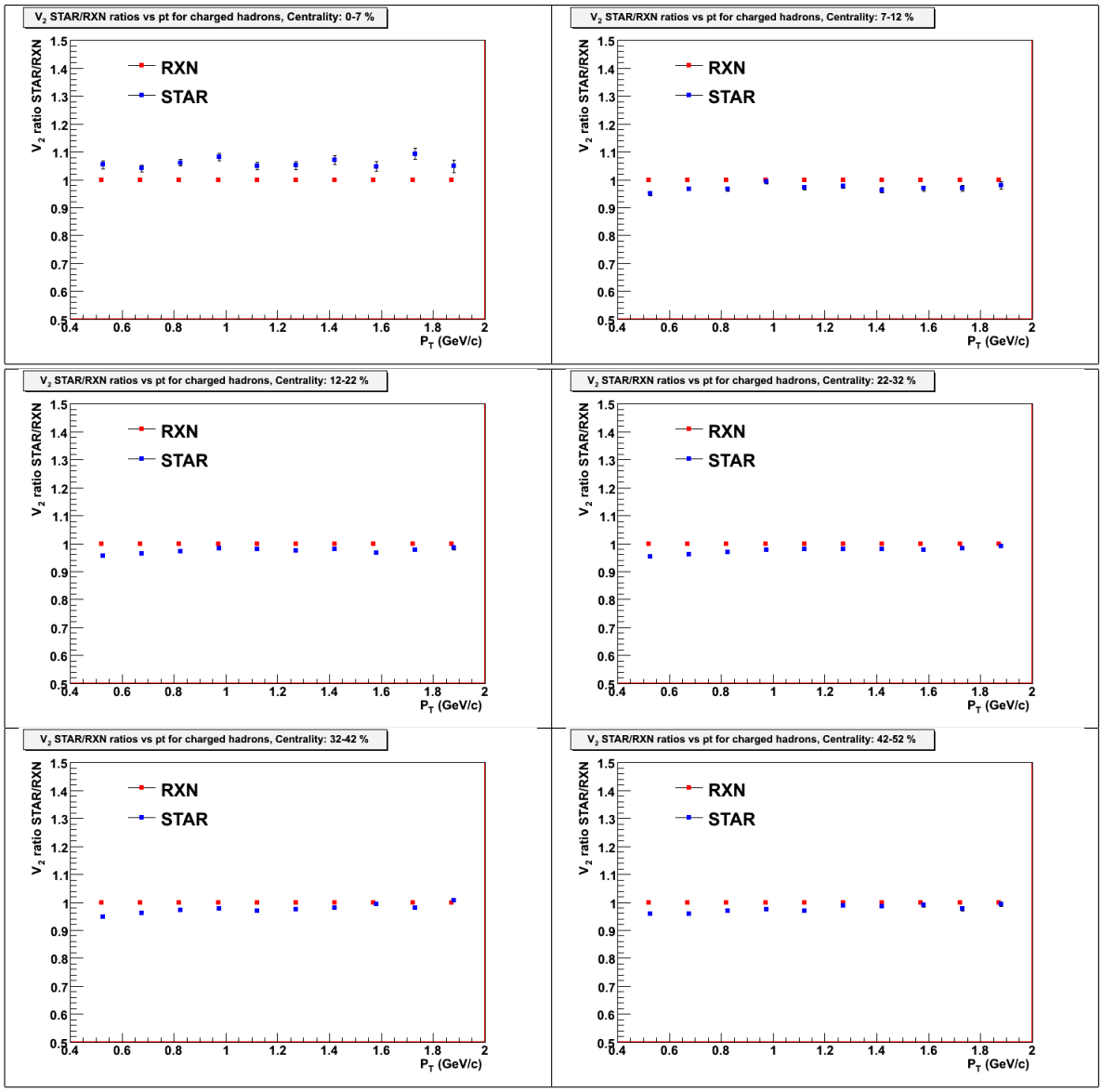

Figure 26: Same as Figure 24, but with 2% centrality shift (0-7-12-...)

6 Conclusion

Azimuthal anisotropy is a powerful tool that can be used to investigate the properties of the medium generated in ultra-relativistic heavy ion collisions. As the azimuthal anisotropy is a product of pressure gradient-driven hydrodynamic flow in the medium, v_2 is expected to be sensitive to the early stages of collision. However, in order to be sure of the meaningfulness of the result, the consistency between different sets of v_2 results need to be checked.

In this work, the magnitude of azimuthal anisotropy, v_2, has been measured for inclusive charged hadrons in Au+Au collisions at $\sqrt{s_{NN}} = 200GeV$ for the centrality range of 0-50% and p_T range of 0.4-1.95 GeV/c. The data used were taken from PHENIX Run 7 of RHIC. The v_2 dependencies on the collision centrality and p_T have been found compatible with our understanding of the collision process. Comparisons have been made between v_2 results measured against event planes obtained by detectors in different pseudo-rapidity ranges (RXN and BBC). It was found that the two sets of results are in close agreement with each other and the differences show no strong dependence on centrality and p_T. Also, comparison has been made with the STAR v_2 results published in the Ref. [8]. The results showed good consistency for the less central events, however, a discrepancy was seen for the most central ones, coming up to as high as 20% difference for the 0-5% centrality bin. There was no strong p_T dependence found for the differences between those two sets of results - the ratios between the two were flat when plotted against p_T. In order to find a way to reconcile the discrepancies seen for the most central collisions, an adjustment of centrality ranges was attempted. It was found that a simple 2% shift in centrality binning brings the two sets of results to an agreement within 5% of each other.

References

[1] A.M.Poskanzer, S.A. Voloshin, Phys.Rev.C58:1671-1678, (1998).

[2] S. Afanasiev et al. (PHENIX Collaboration), Phys. Rev. C 80, 024909 (2009).

[3] A. Adare et al. (PHENIX Collaboration), Phys. Rev. Lett. 98, 162301 (2007).

[4] S. S. Adler et al. (PHENIX Collaboration), Phys. Rev. Lett. 94, 232302 (2005).

[5] S. S. Adler et al. (PHENIX Collaboration), Phys. Rev. Lett. 91, 182301 (2003).

[6] K. Adcox et al. (PHENIX Collaboration), Phys. Rev. Lett. 89, 212301 (2002).

[7] J.-Y. Ollitrault, Eur.J.Phys.29:275-302 (2008).

[8] J. Adams et al. (STAR Collaboration), Phys. Rev. C 72, 014904 (2005).

[9] J. Jia, Doctor thesis, State University of New York at Stony Brook (2003).

[10] M. Shimomura, Doctor thesis, State University of New York at Stony Brook (2009).

[11] A. Taranenko et al., PHENIX Analysis note 869, (2010).

[12] A. Taranenko et al., PHENIX Analysis note 760, (2009).

[13] A. Taranenko et al., PHENIX Analysis note 441, (2005).

[14] A. Tang, Doctor thesis, Kent State University (2002).

[15] B. Yuting, Doctor thesis, NIKHEF and Utrecht University(2007).